eNeuro

Research Article: New Research | Disorders of the Nervous System

High behavioural variability mediated by altered neuronal excitability in *auts2* mutant zebrafish

https://doi.org/10.1523/ENEURO.0493-20.2021

Cite as: eNeuro 2021; 10.1523/ENEURO.0493-20.2021

Received: 17 November 2020
Revised: 25 August 2021
Accepted: 27 August 2021

1. Manuscript Title (50 word maximum)

High behavioural variability mediated by altered neuronal excitability in *auts2* mutant zebrafish

2. Abbreviated Title (50 character maximum)

Escape behaviors in auts2 mutants

3. List all Author Names and Affiliations in order as they would appear in the published article

Urvashi Jha[1,2,5], Igor Kondrychyn[1,5,6], Vladimir Korzh[3,4,7], Vatsala Thirumalai[1*]

[1]National Centre for Biological Sciences, Tata Institute of Fundamental Research, Bellary Road, Bangalore 560065 India.

[2]SASTRA Deemed University, School of Chemical and Biotechnology, Thanjavur, 613401 India.

[3]Institute of Molecular and Cell Biology, 8-13, 61 Biopolis Dr., Proteos, 138673, Singapore.

[4]International Institute of Molecular and Cell Biology, 4 Ks. Trojdena Street, 02-109 Warsaw, Poland.

[5]These authors contributed equally.

[6]Current address: RIKEN Center for Biosystems Dynamics Research, 2-2-3 Minatojima-minamimachi, Kobe 650-0047, Japan.

[7]Current address: International Institute of Molecular and Cell Biology, 4 Ks. Trojdena Street, 02-109 Warsaw, Poland.

4. Author Contributions:

U.J., I.K. and V.T., conception and design; U.J. acquisition and analysis of behavior and imaging data; I.K., generation of the mutant lines; V.K., and V.T., funding acquisition and resources; U.J., I.K. and V.T., drafting the manuscript.

5. Correspondence should be addressed to (include email address)

Prof. Vatsala Thirumalai, National Centre for Biological Sciences, Bellary Road, Bangalore 560065, India. Email: vatsala@ncbs.res.in

6. Number of Figures: 7
7. Number of Tables: 0
8. Number of Multimedia: 3
9. Number of words for Abstract: 246
10. Number of words for Significance Statement: 119
11. Number of words for Introduction: 734
12. Number of words for Discussion: 1165

13. Acknowledgements

The authors would like to thank Mr. T.P. Jagadeesh for maintaining the fish facility

and members of the Thirumalai Lab for helpful discussions.

14. Conflict of Interest
A. No. Authors report no conflict of interest.

15. Funding sources
Wellcome Trust-DBT India Alliance Intermediate and Senior fellowships (VT), Department of Biotechnology (VT), Science and Engineering Research Board, Department of Science and Technology (VT), Department of Atomic Energy (VT-12-R&D-TFR-5.04-0800), CSIR-UGC fellowship (UJ), NCBS Career Development Fellowship (IK). VK's laboratory in the IMCB, Singapore was supported by the institutional grant to the IMCB by the Agency for Science, Technology and Research of Singapore. VK in Poland was supported by the Opus grant of the National Science Foundation (NCN), Poland (2016/21/B/NZ3/00354).

Abstract (250 words)

Autism spectrum disorders (ASDs) are characterized by abnormal behavioral traits arising from neural circuit dysfunction. While a number of genes have been implicated in ASDs, in most cases, a clear understanding of how mutations in these genes lead to circuit dysfunction and behavioral abnormality is absent. The *autism susceptibility candidate 2* (*AUTS2*) gene is one such gene, associated with ASDs, intellectual disability and a range of other neurodevelopmental conditions. Yet, the role of AUTS2 in neural development and circuit function is not at all known. Here, we undertook functional analysis of Auts2a, the main homolog of AUTS2 in zebrafish, in the context of the escape behavior. Escape behavior in wild type zebrafish is critical for survival and is therefore, reliable, rapid, and has well-defined kinematic properties. *Auts2a* mutant zebrafish are viable, have normal gross morphology and can generate escape behavior with normal kinematics. However, the behavior is unreliable and delayed, with high trial-to-trial variability in the latency. Using calcium imaging we probed the activity of Mauthner neurons during otic vesicle stimulation and observed lower probability of activation and reduced calcium transients in the mutants. With direct activation of Mauthner by antidromic stimulation, the threshold for activation in mutants was higher than that in wild type, even when inhibition was blocked. Taken together, these results point to reduced excitability of Mauthner neurons in auts2a mutant larvae leading to unreliable escape responses. Our results show a novel role for Auts2a in regulating neural excitability and reliability of behavior.

Significance statement (120 words):

AUTS2 is one among recently identified autism susceptibility candidate genes, whose function in neuronal circuits is unclear. Using zebrafish as a model organism, we probe the function of Auts2a (homolog of mammalian AUTS2) at the cellular, network and behavioral levels. The escape behavior of Auts2a mutant zebrafish is highly variable with normal short latency escapes, long latency escapes and total failures across trials in the same fish. This occurs because neuronal excitability is inappropriately set in the Mauthner neurons of mutants leading to large trial-to-trial variability in responses. The behavioral variability is fully explained by variability in firing action potentials in the Mauthner neuron, providing an integrative understanding of how behavioral variability arises from mutations at the genetic level.

Introduction (750 words)

Every neuron needs to carefully tune its excitability to be able to perform computation within the circuit in which it is embedded. When firing properties are improperly specified, neuronal function is compromised leading to abnormal behaviors. Transcriptional regulation plays important roles in specifying neuronal excitability properties and therefore, are also a chief class of genes implicated in many neurological diseases including Autism spectrum disorders (ASDs; (Bourgeron, 2015; De Rubeis et al., 2014; Sztainberg and Zoghbi, 2016)). The *autism susceptibility candidate 2* (*AUTS2*, also known as activator of transcription and developmental regulator) gene is a known regulator of transcription in the nervous system (Gao et al., 2014; Russo et al., 2018; Wang et al., 2018) and is associated with several neurodevelopmental disorders including ASD (Beunders et al., 2013; Kalscheuer et al., 2007; Sultana et al., 2002). AUTS2 is expressed in neurons of the central nervous system and is present both in the nucleus and in the cytoplasm (Bedogni et al., 2010; Gao et al., 2014; Hori et al., 2014; Hori and Hoshino, 2017). In the nucleus, AUTS2 binds to members of the Polycomb Repressor Complex 1 (PRC1), but activates transcription of several genes important for neural development and function (Gao et al., 2014; Oksenberg et al., 2014; Wang et al., 2018). In the cytoplasm, AUTS2 regulates the actin cytoskeleton to control neuronal migration and neurite outgrowth (Hori et al., 2014; Hori and Hoshino, 2017). *Auts2* knock-out mice exhibited several deficits such as reduced righting reflexes and ultrasonic vocalizations (Gao et al., 2014). Nevertheless, how AUTS2 controls nervous system development, function and behavioral output are not understood at all.

Previous studies have identified and characterized four paralogs of *auts2* in zebrafish: *auts2a*, *auts2b*, *fibrosin-like 1* (*fbrsl1*) and *fibrosin* (*fbrs*) (Kondrychyn et al., 2017). Both *auts2a* and *auts2b* genes are expressed in the developing and juvenile zebrafish brain. Analysis of gene structure and protein sequence revealed that among the two genes, *auts2a* is the closest orthologue to mammalian *Auts2* (61.58% identity in protein sequence), with even higher homology in the C-terminus, hinting at conserved binding partners and function. In larval zebrafish, *auts2a* is widely expressed in the brain with distinctly high expression in rhombomere 4 (Kondrychyn et al., 2017), which houses neurons of the escape network (Metcalfe et al., 1986).

Teleost escape behavior consists of a sharp C-shaped tail bend away from the inducing stimulus with only a few milliseconds latency (Kimmel et al., 1974; Eaton et al., 1977). The behavior is triggered by action potential firing in one of two bilaterally located giant Mauthner neurons (M-cells) (Eaton and Farley, 1975; Eaton et al., 1977; Korn and Faber, 2005; Kohashi and Oda, 2008; Sillar, 2009). Two pairs of homologous neurons, MiD2cm and MiD3cm, also take part in escape behaviors but fire at much longer latencies (Eaton et al., 1984; Kohashi and Oda, 2008).

Action potential firing in M-cells is required for the fast C-start response (Zottoli, 1977; Eaton et al., 1981). In response to supra-threshold depolarization via strong synaptic inputs or by direct current injection, M-cells in larval and adult zebrafish, as well as adult goldfish, generate a single action potential with a very short latency (Eaton et al., 2001; Nakayama and Oda, 2004; Watanabe et al., 2013). This action potential is conducted quickly via its giant axons to spinal circuitry, including direct synapses onto contralateral motor neurons, resulting in rapid muscle contraction and a sharp bending of the body (Fetcho, 1991). M-cell excitability is thus critical for

quick escape from threatening stimuli. Though not all of the conductances driving M-cell response have been delineated, it is clear that during development, M-cell intrinsic properties are progressively tuned to result in its mature firing behavior (Brewster and Ali, 2013; Watanabe et al., 2017, 2013). Since *auts2a* is expressed in rhombomere 4 at stages when M-cell properties are being defined, we sought to determine how Auts2a impacts excitability of M-cells and therefore the escape behavior itself.

Using customized transcription activator-like effector nucleases (TALENs), we generated mutations in the *auts2a* locus and isolated an allele, which had a premature stop codon in the coding sequence. Using a combination of high-speed videography and *in vivo* calcium imaging, we show that escape behaviors become highly unreliable and slow in *auts2a* mutants and that this unreliability can be explained by the reduced excitability of M-cells. These results indicate a role for Auts2a in regulating neuronal excitability, an action by which Auts2a impacts behaviors significantly.

Materials and Methods

Fish care and use

Zebrafish (*Danio rerio*) of AB strain and Indian wild type were housed in aquarium tanks at 28.5°C with a 14:10 hours light: dark cycle. Fish were maintained according to established protocols as previously described (Westerfield, 2000) in agreement with the Institutional Animal Ethics Committee and the Institutional Biosafety Committee. For fin amputation, fish were briefly anaesthetized in 0.01% Tricaine (MS-222, Sigma-Aldrich), the caudal fin was cut and fish were immediately returned to fresh water. Experiments were performed on 6-8 days post fertilization

(dpf) larval zebrafish at room temperature. Larvae have not undergone sex specification at these stages. Larvae were maintained in 14:10 light: dark cycle at 28°C in E3 medium (5 mM NaCl, 0.17 mM KCl, 0.33 mM $CaCl_2$ and 0.33 mM $MgSO_4$, pH 7.8). Larvae were treated with 0.003% 1-phenyl-2-thiourea in 10% Hank's saline at 24 hpf to remove pigments, for calcium imaging experiments.

TALEN design, construction and synthesis

TALENs specific to *auts2a* were manually designed using criteria as described previously (Bedell et al., 2012) and assembled according to the established protocol (Sanjana et al., 2012). The plasmid kit used for building TALENs was a gift from Dr. Feng Zhang (Addgene kit #1000000019). Once assembled into a destination vector, TALENs were re-cloned into pTNT vector (Promega) containing synthetic polyA tail and T7 terminator sequence. The *auts2a* TALEN recognition sequences are as follows: left TALEN, CCAGCTGGGAGTGCCT and right TALEN, GTAATAGCACTTTAGGTGG. Between the two binding sites is a 16-nt spacer with a *Kpn*I site (ACTCAGgtaccagtca, *Kpn*I site is underlined, intronic sequence is in lower case), facilitating identification of mutations by PCR and *Kpn*I restriction digestion. The spacer region overlaps with the donor splice site at exon 8 (Figure 1A). Capped mRNA was synthesized by *in vitro* transcription using mMESSAGE mMACHINE T7 kit (Invitrogen) and purified with RNeasy Mini kit (Qiagen). Zebrafish embryos at the 1-cell stage were microinjected with 200 pg RNA (100 pg each of left and right TALEN mRNA). At such a dose, over 70% embryos survived and showed TALEN-induced somatic *auts2a* gene modifications.

204

205 **DNA isolation and genotyping**

206 Genomic DNA was isolated from either embryos or fin clips using HotSHOT method
207 (Meeker et al., 2007). One microliter solution was then used in a 25 µL PCR
208 containing the following reagents at these concentrations: 200 nM each gene-
209 specific primers (forward 5'-TCAGCGAACCCTACAGCTTCACACA-3' and reverse
210 5'-TGGGGTACGCACCATGGGCGGTGCA-3'), 0.2 mM dNTPs, 1x PCR buffer and
211 0.625 units One*Taq* HotStart DNA polymerase (New England BioLabs). Reaction
212 was amplified using the following conditions: 94°C for 1 min; 40 cycles of 94°C for 20
213 s, 68°C for 1 min; followed by 68°C for 1 min. PCR products were purified using PCR
214 purification kit (Qiagen) and digested with restriction enzyme *Kpn*I-HF (New England
215 BioLabs) at 37°C for 60 min. The resulting reactions were loaded onto a 1.8%
216 agarose gel and electrophoresed in 1x Tris-acetate-EDTA (TAE) buffer. Mutations
217 were assessed by loss of restriction enzyme digestion. To verify mutations, the gel
218 purified uncut PCR products were cloned into pCRII-TOPO vector (TOPO TA
219 Cloning kit, Invitrogen) and sequenced.

220

221 **RT-PCR and RNA isolation**

222 Total RNA was isolated from wild type and *auts2a*^{ncb104} heterozygote and
223 homozygote embryos using an RNeasy Mini kit (QIAGEN), and first-strand cDNA
224 was synthesized from 1 µg of total RNA by oligo(dT) priming using SMARTScribe
225 Reverse Transcriptase (Clontech) according to the manufacturer's protocol.
226 Amplification of cDNA was performed using Herculase II Fusion DNA polymerase
227 (Agilent). Identity of amplified PCR products was verified by direct sequencing.

228

Whole-mount Immunohistochemistry

Embryos were fixed in 4% PFA at 4°C overnight, washed 3 times for 15 min in PBST (1 x PBS, 0.1% Tween-20) and permeabilized in 0.1% Triton X-100 in 0.1% sodium citrate for 30 min at 4°C. Then embryos were incubated for 2 hours in 5% Blocking Reagent (Roche) in MAB (150 mM maleic acid, pH 7.5, 100 mM NaCl, 0.1% Tween-20) at room temperature. Embryos were incubated with 3A10 antibodies (DSHB, 1:200) overnight at 4°C, washed 4 times for 30 min in MAB and incubated with HRP-conjugated goat anti-mouse $F(ab)_2$ fragments (Molecular Probe, 1:500) for 6 hours at room temperature or overnight at 4°C. Embryos were extensively washed in PBST, stained with 3,3'-diaminobenzidine (DAB) and washed several times in PBST. Embryos were kept in 50% glycerol in PBS at 4^0C until further imaging.

Head restrained preparation

For behaviour and calcium imaging experiments, larvae were embedded in 2% low gelling agarose (Sigma-Aldrich, Missouri, USA). E3 medium was added after the agarose congealed. Agarose around the tail and the OV were removed for observing tail movements and application of water pulse for behavioral experiments.

High-speed recording of escape response

Escape responses were evoked by applying a water pulse to the OV or to the tail at the level of cloaca, with a glass capillary (tip diameter 0.05-0.06 mm) mounted on a micromanipulator (Narishige; Tokyo, Japan). The water pulses were generated by a pressure pulse of 10 ms duration and pressure of 30 psi from a microinjection dispense system (Picospritzer III, Parker Hannifin, Ohio, USA). Videos were

acquired at 1000 fps with a high-speed camera (Phantom Miro eX4, Vision research, New Jersey, USA) mounted on a stereo microscope (SZX16, Olympus, Tokyo, Japan) at 512 x 512 pixel resolution and 500 µs exposure time. Methylene blue (1%) was used to visualize the water jet for tracking its contact with the larva. Six trials (three on each side) were performed on each larva.

Retrograde labelling of Mauthner neurons

Mauthner neurons were retrogradely labelled with fluorescent calcium indicator Oregon Green Bapta-1 dextran, 10000 MW (Invitrogen, California, USA) or Calcium Green dextran, 10000 MW (Invitrogen, California,USA) for calcium imaging experiments. For Mauthner and its homologs imaging, neurons were retrogradely labelled with Tetramethylrhodamine dextran,1000 MW (Invitrogen). Larvae were first anaesthetised in 0.01% MS-222 (Sigma Aldrich; Missouri,USA) in E3 medium. 25% OGB-1/CGD/TMR-dextran in 10% Hank's Balanced Salt Solution (HBSS; 137 mM NaCl, 5.4 mM KCl, 0.25 mM Na_2HPO_4, 0.44 mM KH_2PO_4, 1.3 mM $CaCl_2$, 1.0 mM $MgSO_4$, 4.2 mM $NaHCO_3$) was pressure injected with a glass microcapillary into the spinal cord (at the level of cloaca) using a Picospritzer. Post injection, larvae were allowed to recover in HBSS for >12h.

Electrical stimulation

Electric shock stimuli (40 µA, 1 ms) were delivered using a bipolar electrode (FHC, Bowdoin, ME, USA) placed at the OV. The pulse was generated using ISO-Flex stimulus isolator (A.M.P.I., Jerusalem, Israel), triggered by pClamp (Molecular devices, California, USA). For antidromic stimulation of the M-axon, larvae were anaesthetized in 0.01% MS-222 (Sigma-Aldrich; Missouri, USA) and were pinned

down through notochord using fine tungsten wire (California Fine Wire). The MS222 was then replaced by external solution (composition: 134 mM NaCl, 2.9 mM KCl, 1.2 mM $MgCl_2$, 10 mM HEPES, 10 mM glucose, 2.1mM $CaCl_2$, 0.01 mM D-tubocurarine; pH 7.8; 290 mOsm) and skin along the tail was carefully removed using forceps (Fine Science Tools, Foster City, USA). Muscles in a hemi-segment (between the 10^{th} and 13^{th} myotomes) were carefully removed to expose the spinal cord. The bipolar electrode was placed on top of the exposed spinal segment and brief electrical stimuli of increasing strengths (10 µA onwards, 1 ms in duration) were delivered.

Calcium imaging

Calcium activity upon electrical stimulation of OV/M-axon, in retrogradely labelled Mauthner neurons, was imaged at 35-51 frames per second using an EMCCD camera (Evolve, Photometrics, UK) mounted on a compound microscope (BX61W1, Olympus, Tokyo, Japan) with a water-immersion objective (LUMPlanFL 60X) and Image-Pro Plus (Media Cybernetics, UK) acquisition software.

Drugs

50 µM of strychnine (Sigma-Aldrich) and 100 µM gabazine (Sigma-Aldrich) were dissolved in external solution. Measurements were taken after two minutes of drug application.

Analysis

Data were analysed using MATLAB (Mathworks; Massachusetts, USA) and Fiji (NIH).

304

305 **Behavioural analysis**

306 Latency was defined as the time taken from when the water jet made contact with
307 the larva to the first visible tail contraction. Tail bend angle was calculated by
308 measuring the angle formed by joining a straight line passing through the tail at
309 maximum bend and a straight line passing through the head and the tail in a pre-
310 stimulus frame (Figure 2C). Escape responses were defined as contralateral tail
311 bends with latency ≤100 ms (Kimmel et al., 1974; Kohashi and Oda, 2008). Tail
312 bend responses with latency >100 ms or no observable tail bend upto 1 s post
313 stimulus delivery were classified as failures ('no response').

314

315 **Calcium activity analysis**

316 Relative changes in fluorescence from resting (ΔF/F) were calculated post
317 background and movement correction. Activity in Mauthner neurons was considered
318 to have occurred only for ΔF/F traces with minimum peak ΔF/F of 0.1 for OGB-1
319 dextran and 0.05 for CGD and full width at half maximum of at least 1 s. Threshold
320 for antidromic stimulation of Mauthner was defined as the minimum stimulus intensity
321 at which the Mauthner neuron showed calcium activity for at least 3 of 5 trials at the
322 given stimulus intensity.

323

Dendritic length and **soma volume** were measured using simple neurite tracer and volume viewer plugins in Fiji (Schindelin et al., 2012). Dendritic length of the homologs could not be measured because of inadequate labelling given their small size.

Statistics

Data were tested for normality using one sample Kolmogorov-Smirnov test ($p<0.05$) and equality of variance with *F* test ($p<0.05$). Two sample *t*-test or Mann-Whitney U test were performed for comparisons between two groups and Kruskal-Wallis test was used for comparing three groups. Chi-square test was performed for comparison of proportions.

Results

Generation of the *auts2a* knockout zebrafish line

A pair of TALENs were designed to target the donor splice site at exon 8 of the *auts2a* gene (Figure 1A). The TALEN-targeted sequences surround a restriction enzyme site for easy screening through introduction of a restriction fragment length polymorphism. We identified 5 different mutant alleles (Figure 1A), 3 of which led to a frameshift after S498 and premature stop codons after several missense amino acids (Figure 1B) and one of them, *auts2a*^{ncb104}, was selected to establish an *auts2a* KO zebrafish line. This line harbours a 11-nt deletion, which disrupts the donor splice site affecting correct splicing between exon 8 and exon 9. RT-PCR analysis of RNA isolated from homozygotes revealed that *auts2a*^{ncb104} pre-mRNA uses two alternative cryptic donor splice sites found in the intron in order to splice exon 8 to exon 9 (Figure 1A, B). As a result, the intronic sequence is partially retained in

348 *auts2a*^{ncb104} mRNA leading to a premature stop codon at amino acid 504 after 6
349 missense amino acids (Figure 1B).

350 The zebrafish Auts2a protein has several domains, previously predicted in
351 human AUTS2 (Sultana et al., 2002): two proline-rich (PR) regions, PR1 at amino
352 acids 273-492 and PR2 at amino acids 558-656, PY (PPPY) motif at amino acids
353 524-528, and the Auts2 family domain at amino acids 660-882 (Figure 1B). In
354 Auts2a^{ncb104}, only the PR1 region is retained (Figure 1B). The zebrafish *auts2a* gene
355 locus shows tremendous transcriptional complexity with multiple isoforms generated
356 via alternative splicing and alternative promoter usage (Kondrychyn et al., 2017).
357 Exon 8 is a common exon in all isoforms (Figure 1-1A) and in *auts2a*^{ncb104} mutant all
358 isoforms will be similar affected: a loss of the C-terminal portion of Auts2a,
359 comprising PY motif, PR2 region and the Auts2 family domain (Figure 1-1B).

360

361 **_auts2a_ mutants display high variability in escape responses**

362 *Auts2a* KO zebrafish showed normal development and gross morphology
363 (Figure 2A). *auts2a*^{ncb104} homozygote fish did not show significant difference in size
364 (Mean±S.D. (mm): Wild type, 5.0±0.1(24 larvae); Mutants, 4.9±0.2 (24 larvae);
365 p=0.37; Mann-Whitney test. Moreover, *auts2a*^{ncb104} homozygote fish survive to
366 become fertile adults. As *auts2a* is a neurodevelopmental gene (Oksenberg and
367 Ahituv, 2013) and is expressed at very high levels in rhombomere 4 (Kondrychyn et
368 al., 2017), which houses the escape network, we first investigated whether M-cells,
369 the command-like neurons driving escape behavior, are present in *auts2a* mutants.
370 Wild type larvae possess a single pair of M-cells that send commissural axons down
371 the spinal cord (Fetcho, 1991). In *auts2a* mutants both M-cells are present and send
372 commissural axons (Figure 2B). However, M-cells in *auts2a* mutants were smaller:

both soma volume and dendritic length were significantly reduced (Figure 2C-D). No significant difference in soma volume was observed for the M-cell homologs (Figure 2 C, E). This suggests possible effects on M-cell function leading to deficits in escape behavior.

Next, we asked if *auts2a* mutants exhibited any deficits in escape behavior. We evoked the C-start escape behavior in partially restrained zebrafish larvae between 6-8 days post fertilization (dpf), by directing a strong jet of water at the otic vesicle (OV) (Figure 3A). The restrained preparation ensures similar location of water jet delivery across larvae. The C-start escape response consists of a large angle contralateral tail bend initiated within 3-13 ms of stimulus delivery (Figure 3B). We measured three parameters associated with the C-start escape response: the probability of initiating escapes (% trials where escapes were observed), the latency (time from stimulus arrival at the OV to movement onset) and the maximum tail bend angle, in wild type, heterozygotes and *auts2a* mutant larvae. First, *auts2a* mutants showed a higher percentage of failures to initiate escape responses compared to heterozygotes and wild type larvae (Figure 3C). While wild type and heterozygote larvae showed a contralateral tail bend response in nearly 98% of trials, *auts2a* mutants were able to generate escapes in only 76% of trials. Mutants also had increased probability of failures (no tail bend response) compared to heterozygote and wild type larvae. Next, we asked if the increased failure rates observed in mutants was due to few individuals that did not respond across any of the trials. Surprisingly, we observed that individual larvae displayed highly variable responses across trials (Video 1). Figure 3D shows responses from 5 wild type and 5 mutant larvae across 6 trials. While all wild type larvae were able to initiate escape responses within 10-20 ms, 4 of 5 *auts2a* mutants showed failures in at least one

trial. In addition, the latency to initiate escapes was longer and more variable in mutants compared to wild type (Range: 3-552 ms; Figure 3D, E). Escape response can be generated via multiple pathways. While fast escape responses to head directed stimuli result from activation of the M-cells and its segmental homologs (M-series) (Kohashi and Oda, 2008; Liu and Fetcho, 1999), neural circuitry underlying long-latency escape responses is less well understood (but see (Marquart et al., 2019). Therefore, we next compared latencies of the fast escape response (cut-off latency: ≤20 ms) between wild type, heterozygotes and *auts2a* mutants. Fast escape responses in *auts2a* mutants occur at longer latencies compared to wild type (Figure 3F). Further, the coefficient of variation (CV) of latencies for individual larvae across successive trials was significantly higher for the mutant group in comparison to wild type larvae (Figure 3G). Nevertheless, the kinematics of the escape response were not affected in mutants, as evidenced by the similar maximal tail bend angles observed (Figure 3H). Thus, initiation of tightly regulated, high performance escape response is unreliable and slow in *auts2a* mutants.

Escape response defects in *auts2a* mutants persist on changing the location of sensory stimulation

Stimulation of the OV with water jet activates the M-cell and its homologs, while the same stimulus applied to the tail activates the M-cell alone (O'Malley et al., 1996; Liu and Fetcho, 1999). To investigate if M-cell mediated escapes are compromised in *auts2a*^{ncb104} larvae, we applied the water jet to the tail at the level of the cloaca (Figure 4A, B). In wild type larvae, tail stimulation with water pulse resulted in fast escape responses with characteristic short latency and contralateral

tail bend in 76% trials (Figure 4B,C). Similar to OV stimulation, *auts2a* mutants displayed a high percentage of failures in escape response but similar percentage of ipsilateral tail bend responses to wild type (Figure 4C). Tail stimulation also resulted in significantly longer latencies in mutants than in wild type larvae (Figure 4D). However, no significant difference was observed in the CV of latencies across trials in an individual larva between wild type and mutants (Figure 4E). This result indirectly implies that the increased CV in latencies seen with the head stimulation of auts2a mutants (Figure 3G) is contributed by deficits in M-cell homologs. No difference was observed in tail bend angles between wild type and mutant groups (Figure 4F).

Mauthner neuron fails to fire reliably in *auts2a* mutants

To directly assess M-cell firing in *auts2a* mutants, we next monitored calcium activity in OGB-1 dextran labelled M-cells upon electrical stimulation of OV (Figure 5A). OV stimulation resulted in a large increase in fluorescence from rest (Figure 5B, C, Video 2) and this response was evoked reliably in wild type larvae (Figure 5B-D). Mutants displayed a greater proportion of failures in calcium response (Figure 5B-D, Video 3). Mutants also showed lower peak calcium signals compared to wild type (Figure 5C, E). In addition, the CV of the peak calcium response was not statistically different between wild type and mutant larvae (Figure 5F). This implies that the increased variability in latency seen with OV stimulation (Figure 3G) does not arise from variability in the response of the M-cell itself.

Mauthner neurons in *auts2a* mutants have reduced excitability

Failures in calcium activity response in the mutants after OV stimulation could result either from reduced excitability of M-cells and/or defects in sensory processing involving mechanosensory hair cells and the VIIIth cranial nerve. To ascertain the role of the M-cells, we stimulated its axon (antidromic stimulation) which resulted in calcium activity transients similar to OV stimulation (Figure 6A).

Due to the large diameter of the M-cell axon, it has the lowest threshold for extracellular stimulation (Kimmel et al., 1982). At low stimulation intensity other cells are unlikely to be activated, making the stimulation M-cell-specific. We defined the threshold intensity as the minimum stimulus intensity at which calcium signals were evoked in the M-cell in at least 3 out of 5 trials (Figure 6B). Compared to wild type, threshold intensity was significantly higher in *auts2a* mutants (Figure 6C-D). However, at intensities equal to or higher than threshold, M-cells responded reliably in both mutants and wild type larvae (Figure 6E) and the peak calcium signal was significantly reduced in mutants compared to wild type larvae (Figure 6F, G), similar to that seen after OV stimulation (Figure 5E).

Alternatively, the increased threshold to fire in M-cells could result from increased inhibition upon them. To rule out this possibility, we next performed antidromic stimulation before and after application of strychnine and gabazine to block glycine receptors and GABA-A receptors respectively (Roy and Ali, 2014; Takahashi et al., 2002). Application of these antagonists did not alter the threshold intensity (Figure 6H) or peak $\Delta F/F$ (Figure 6I) in the wild type or auts2 mutant larvae. These results show that the increased failures, latency and variability in latencies all derive from increased threshold to fire M-cells.

Discussion

We show that auts2a mutant zebrafish exhibit interesting deficits in escape response: the response probability and latency are highly variable across trials in individual mutant larvae. As a consequence of *auts2a* mutation, reliable firing of M-cells is lost and therefore, escape responses become unreliable also. To explain the behavioral variability, we propose that in trials where the M-cell fires, normal short latency escape is triggered; in trials where neither the M-cell nor its homologs fire, fish fail to generate escape responses; and in trials where only the homologs fire, the latency to respond is much longer (Figure 7). We confirmed the hypoexcitability of the mutant M-cells by directly stimulating the M-axon. Mounting an appropriate and fast escape response reliably is essential for survival and thus Auts2a serves an essential function for the animal. We also observed reduced peak $\Delta F/F$ calcium response in the mutants. As calcium response upon antidromic stimulation of M-cells reflects calcium influx via voltage-activated calcium channels (Takahashi et al., 2002), the reduced peak calcium response could result from deficits in the number or activation of these channels in the mutants.

We also showed that somata and dendrites of auts2 mutant M-cells are smaller compared to wild type. M-cells receive dense synaptic input on their dendrites and reduction in dendritic size may lead to decrease in synaptic drive. The smaller size of the cells may lead to reduced channel conductances, and/or reduced synaptic drive. In addition, global auts2 knock-out, as was done in this study, is indeed likely to result in widespread changes both within the escape network and outside. Nevertheless, given that we see longer, more variable escape latencies and a consistent increase in the threshold of M-cell firing in the auts2 mutants, we can conclude that these specific deficits in the short latency escape behavior are due to the hypoexcitability of the M-cell.

The escape circuit as a model circuit for testing gene function

The escape system in zebrafish has been an advantageous tool for dissecting the genetic underpinnings of behavior, learning and decision-making (Gahtan and Baier, 2004; Wolman and Granato, 2012). Forward genetic screens identified mutants with specific deficits in generating escapes such as the *twitch twice* and *space cadet* mutants (Burgess et al., 2009; Granato et al., 1996; Lorent et al., 2001). More recent studies have reported mutants with deficits in sensitivity (Marsden et al., 2018), habituation (Wolman et al., 2015), pre-pulse inhibition (Burgess and Granato, 2007) or in deciding between Mauthner-mediated short latency escapes and non-Mauthner mediated long latency escapes (Jain et al., 2018). The specific defects identified in these studies range from errors in axon guidance, extracellular calcium sensing and IGF signaling in M-cells and other members of the escape circuit. Our study makes an important addition to these studies by identifying Auts2a to be a direct genetic determinant of excitability in M-cells.

M-cells are specified soon after gastrulation and evoke escape responses to touch in larvae as young as early as 2 dpf (Kimmel et al., 1974; Kohashi et al., 2012). As the larvae mature, M-cells drive startle behaviors in response to auditory/vestibular stimulation as well. Concomitant with these changes, the firing behavior of M-cells changes from firing multiple action potentials upon reaching threshold to firing only a single action potential after 4 dpf. This change in firing behavior of the M-cells drives maturation of the escape behavior from one involving multiple C-bends to that with only a single C-bend followed by routine swimming. The alteration in M-cell firing behavior is in part due to the expression of distinct types of potassium channels including those that are sensitive to dendrotoxin

(Watanabe et al., 2013, 2017). These studies underline the critical importance of regulating the intrinsic properties of M-cells for generating appropriate C-start behaviors. Hyperexcitability will result in multiple C-starts while hypo-excitability in M-cells and its homologs, as seen in *auts2a* mutants, will lead to failures in escapes.

Mechanism of action

ChIP-seq analysis revealed that in the mouse brain, AUTS2 binds preferentially to promoter and enhancer regions of genes involved in nervous system development (Gao et al., 2014; Oksenberg et al., 2014). In mouse forebrain alone, 784 AUTS2 binding sites were in promoter regions and 1146 sites were distal to promoter regions. Regardless of whether the sites were within promoter regions, these AUTS2 binding sites were found to be associated with genes implicated in ASDs. Further, binding of AUTS2 to these sites seems to activate their expression resulting in higher transcript levels. Importantly, among the targets of AUTS2 binding are genes associated with intracellular calcium homeostasis such as pumps and transporters, voltage-gated calcium channels and sodium channels, potassium channels as well as synaptic receptors (Oksenberg et al., 2014). If these targets are conserved in zebrafish as well, loss of Auts2a might interfere with expression levels of one or more of these targets leading to hypoexcitability of M-cells.

Manipulations that reduce global activity levels of neurons in culture lead to homeostatic resetting of intrinsic and synaptic properties (Turrigiano et al., 1998; Desai, 2003; Turrigiano and Nelson, 2004), a process that requires transcription (Ibata et al., 2008). Recently, it was shown that manipulations that induce homeostatic plasticity also trigger significant upregulation of AUTS2 expression (Schaukowitch et al., 2017). Thus, on the basis of our study and these earlier

studies, we propose that Auts2 is important for setting and maintaining the excitability set-points of neurons.

Alterations in neuronal excitability and ASDs

Since ASDs are frequently also comorbid with epilepsy, and because mutations that reduce inhibition or increase excitation frequently associate with them, ASDs were initially thought to result from hyperexcitation in the central nervous system (Rubenstein and Merzenich, 2003). However, it is becoming clear that balance between excitation and inhibition is key and when that balance is tilted towards more excitation or more inhibition, network function is impaired leading to ASD-like phenotypes (Nelson and Valakh, 2015; Lee et al., 2017; Sohal and Rubenstein, 2019). Activity imaging using expression of the immediate early gene *c-Fos* reveals hypoactivity in much of the forebrain in a mouse model of Rett syndrome (Kron et al., 2012). Reduced connectivity and reduced activation of forebrain structures at rest have also been reported in fMRI studies of human autistic subjects (Minshew and Keller, 2010). These studies underline the fact that since ASDs are associated with mutations in multiple genetic pathways, they should be thought of as diseases resulting from abnormal excitation to inhibition balance. Consistent with this view, a recent study demonstrates that in *Auts2* mutant mice, hippocampal pyramidal neurons receive increased excitatory synaptic inputs with no change in the amount of inhibition received, upsetting the excitation to inhibition balance (Hori et al., 2020). We have shown that loss of function of Auts2a in zebrafish leads to hypoexcitability in an identified neuron, the M-cell, which is responsible for driving fast escapes. Further, we showed that the hypoexcitability is not due to altered inhibition to the M-

cells. Auts2a might affect M-cell firing by acting on its intrinsic properties and the targets remain to be identified in future studies.

Figure legends

Figure 1. TALEN-induced mutation in the *auts2a* gene.

(A) Zebrafish *auts2a* gene locus, TALEN target sites and isolated alleles. The TALENs target a pair of binding sites (in blue) flanking a spacer with a restriction enzyme site (in green). Exonic and intronic sequences are shown in upper and lower cases, respectively. In contrast to genomic sequence annotated in the Ensembl (WT), our "in-house" zebrafish AB strain (WT^{*}) has a polymorphism in intronic sequence adjacent to exon 8 (in red). Alleles *ncb101*, *ncb103*, *ncb104* and *ncb105* have the nucleotide deletions that disrupt the donor splice site (in bold) leading to a frameshift after S498 and premature stop codons. Deletion in allele *ncb102* does not affect correct splicing and the Auts2 protein sequence. Three single point mutations were introduced in the intron of $auts2a^{ncb104}$ allele (in orange) leading to a stop codon creation (underlined). The alternative donor splice sites used to splice mutant $auts2a^{ncb104}$ pre-mRNA are highlighted in grey.

(B, top) Auts2a and $Auts2a^{ncb104}$ proteins. The *ncb104* mutation causes the loss of the C-terminal portion of Auts2a, comprising PY motif, proline-rich region PR2 and the Auts2 family domain. **(B, bottom left)** RT-PCR analysis of *auts2a* mRNA, isolated from wild type (WT), *ncb104* heterozygote (HET) and homozygote (MUT) embryos. M, 100-bp DNA ladder (NEB). **(B, bottom right)** Partial protein sequences of mutant alleles. See also Extended Data Figure 1-1.

Figure 1-1: $Auts2a^{ncb104}$ allele in different auts2a isoforms.

A. Overview of transcripts generated from the auts2a gene (modified from Kondrychyn et al. 2017). Noncoding and coding exons are depicted as open and filled bars, respectively. Alternative transcription start sites are used to generate

auts2a isoforms. B. Schematic structure of Auts2a^{wt} and Auts2a^{ncb104} proteins translated from the different auts2a isoforms. Positions of coding exons are marked for the reference (relative exon size is not in scale). Missense amino acids preceding premature stop codon are shown in red. Exons 1B and 1D code the alternative N-terminal amino acids. PR1 spans exons 7 and 8, PR2 spans exons 9-13 and the Auts2 family domain spans exons 14-19.

Figure 2. Morphological characterization of auts2a mutants

(A) Bright field images of wild type and homozygote larvae. Scale bar represents 2 mm.

(B) Whole mount immunostaining with 3A10 antibody at 30 hours post fertilization (hpf) in *auts2a* mutants. Arrowhead points to the cell body of the Mauthner neuron and arrow points to the axon.

(C) Maximum intensity Z-projection of Mauther neuron (top) and homologs (bottom) of wild type (left) and mutant (right) larvae. Scale bar: 10 µm.

(D) Comparison of Mauthner lateral dendrite lengths in wild type and *auts2a* mutant larvae.

(E) Comparison of Mauthner soma volume in WT and mutant larvae. n_{WT} = 8 cells from 7 larvae; n_{mut} = 15 cells from 12 larvae. *p<0.05; Mann-Whitney U test.

(F) Comparison of soma volume of the M-cell homologs. n_{WT} = 7 cells from 5 larvae; n_{mut} = 14 cells from 12 larvae. ns, not significant; Mann-Whitney U test.

Figure 3. Onset of escape response is delayed and highly variable in *auts2a* mutants.

(**A**) Schematic of experimental set up. Escape response was evoked in zebrafish larvae (6-8 dpf) by directing a strong water-jet at the otic vesicle (OV). Escape response is characterised by a large angle tail deflection, contralateral to the direction of water-jet.

(**B**) Time lapse of escape response. 1. Pre-stimulus frame. 2. Water jet makes first contact with OV. 3. First visible tail contraction (marked with asterisk). 4. Representative frame showing references used for maximum tail bend angle calculation.

(**C**) Pie chart showing percentage of contralateral, ipsilateral and no tail bend responses observed across wild type (n=143 trials), heterozygotes (n=258 trials) and *auts2a* mutants (n=371 trials). Chi-square test.

(**D**) Escape latencies across successive trials from five wild type and mutant larvae. Color bar represents escape latencies. NR: no response.

(**E**) Comparison of escape response latencies in wild type (WT), heterozygotes (HET) and *auts2a* mutants (MUT). n_{WT}=140 trials from 24 larvae, n_{HET}=254 trials from 43 larvae and n_{MUT}=292 trials from 57 larvae.

(**F**) Cumulative density function plot for short-latency escapes (latencies ≤ 20 ms) in wild type (n=140 trials), heterozygotes (n=254 trials), and *auts2a* mutants (n=273 trials).

(**G**) Coefficient of variation of latencies across successive trials in individual larvae for wild type (n=24), heterozygotes (n=43) and mutants (n=53) groups.

(**H**) Comparison of maximum tail bend angle of contralateral turns between the three groups (n=140 trials, WT; n=254 trials, HET; n=281 trials, mutants).

649 Kruskal Wallis; Mann-Whitney test for between-groups comparisons with Bonferroni
650 correction for multiple comparisons. *p<0.025, **p<0.005, ***p<0.0005; ns, not
651 significant.
652
653 **Figure 4. Escape response defects in *auts2a* mutants persist on changing the**
654 **location of sensory stimulation**
655 **(A)** Schematic of experimental set up.
656 **(B)** Time lapse of escape response evoked by tail stimulation. 1. Pre-stimulus frame.
657 2. Water jet makes first contact with the tail. 3. First visible tail contraction (marked
658 with asterisk). 4. Representative frame for maximum tail bend angle calculation.
659 **(C)** Pie chart showing percentage of contralateral tail bends, ipsilateral tail bends and
660 failures to initiate an escape response between wild type (n=92 trials) and mutants
661 (n=113 trials) .
662 **(D)** Comparison of escape response latencies on tail stimulation between wild type
663 (n=71 trials,16 larvae) and *auts2a* mutants (n=67 trials,19 larvae).
664 **(E**) Comparison of coefficient of variation of latencies across successive trials for
665 each larva between wild type (n=17) and mutant (n=18) groups.
666 **(F)** Maximum tail bend angle of turns for WT (n=72 trials) and mutants (n=72 trials).
667 *p<0.05, ***p<0.0001; ns, not significant.
668
669 **Figure 5. Mauthner neuron fails to fire reliably in *auts2a* mutants**
670 **(A)** Schematic representation of experimental set up. Mauthner
671 neuron was retrogradely labelled with OGB-1 dextran and calcium activity was
672 monitored upon electrical stimulation (40 µA, 1ms) of OV.

673 **(B)** Left: Raster plot of all trials in WT (n=68 trials; 10 larvae) showing consistent
674 calcium activity across several trials on OV stimulation.
675 Right: Calcium responses observed across all trials in the mutant group (80 trials; 14
676 larvae). White line represents the time of stimulus delivery.
677 (C) Top: ΔF/F profile of a Mauthner neuron in an example wild type larva across 8
678 trials in response to electrical stimulation of the OV. Bottom: ΔF/F profile of a
679 Mauthner neuron in an example *auts2a* mutant larva showing sub-threshold
680 response as well large calcium transients across 8 trials upon electrical stimulation of
681 OV.
682 (D) Probability of calcium activity response across trials per larva (n_{WT}=10 larvae,
683 n_{MUT}=14 larvae).
684 (E) Peak ΔF/F in WT and mutants (n_{WT}=68 trials, n_{MUT}= 80 trials).
685 (F) Comparison of coefficient of variation of peak ΔF/F between wild type and mutant
686 larvae.
687 Mann-Whitney U test; ***p<0.0001.
688
689 **Figure 6. Mauthner neuron in *auts2a* mutants have reduced excitability**
690 **(A)** Schematic of experimental set-up. Calcium activity in the Mauthner neuron was
691 observed on antidromic stimulation. Mauthner neuron was retrogradely labelled with
692 OGB-1 dextran.

693 **(B)** ΔF/F profile for an example wild type larva upon antidromic stimulation with 10μA
694 (left) and 20 μA (right) stimulus intensity. Mauthner neuron fired reliably at the
695 threshold intensity of 20 μA .
696 (**C**) Representative raster plot from a wild type larva (left) and mutant larva (right)
697 Each row represents average ΔF/F over five trials at the respective stimulus
698 intensity. The threshold for calcium activity for wild type larva is 20 μA whereas for
699 the mutant larva is 70 μA.
700 (**D**) Normalised histogram of calcium activity threshold for WT (n=9 larvae) and
701 *auts2a* mutants (n=12 larvae).
702 **(E)** Summary data of probability of calcium activity at 0.5x, 1x, 1.5x threshold
703 stimulus intensity for wild type and mutant group.
704 **(F)** ΔF/F profiles for a representative wild type larva (black) and a mutant larva (red)
705 on antidromic stimulation. Shaded regions represent SEM from five trials.
706 **(G)** Summary data of peak calcium signal in wild type (n=45 trials, 9 larvae) and
707 *auts2a* mutants (n=60 trials, 12 larvae).
708 *p<0.05, **p<0.001; Mann-Whitney U test
709 **(H)** Calcium activity threshold for wild type (n=9) and mutant (n=7) larvae before and
710 after bath application of 50 μM strychnine and 100 μM gabazine. Mauthner neurons
711 were labelled with calcium green dextran for this experiment. Wilcoxon signed rank
712 test.
713 **(I)** Peak ΔF/F for wild type (n=9) and mutant (n=7) larvae before and after bath
714 application of 50 μM strychnine and 100 μM gabazine. Paired sample t-test.

Figure 7. Summary of behavioural abnormalities in escape response in *auts2a* mutants.

Top: In response to threatening stimuli, the ipsilateral Mauthner neuron and its homologs in the hindbrain (marked in a dashed box) fire reliably (yellow) resulting in short latency escape responses across consecutive trials (left to right) in wild type larvae.

Bottom: In auts2a mutants, Mauthner neurons fire unreliably. This means that on some trials, larvae exhibit normal short latency escapes when the Mauthner neuron is able to fire (left). On trials, where the Mauthner fails to fire, long latency escape responses may be initiated perhaps due to the activation of homologs (middle) and if neither the Mauthner, nor the homologs fire, then the larvae fails to respond (right). "?" denotes putative activity in Mauthner homologs during Mauthner mediated and Non-Mauthner mediated escapes.

730 Table 1- Statistics
731

Figure Number	Data Structure	Type of test	Statistics
Figure 2D	Non-normal	Mann-Whitney U test	p = 0.0219 for differences in dendritic length between wild type and mutants
Figure 2E	Non-normal	Mann-Whitney U test	p = 0.0420 for differences in soma volume between wild type and mutants
Figure 2F	Normal	t-test	p=0.679 for differences in soma volume of homologs between wild type and mutants
Figure 3C	-	Chi-square test	p =6.5630e-09 and p= 6.2760e-15 for differences in contralateral tail bend between wild type and mutants and heterozygotes and mutants respectively
Figure 3C	-	Chi-square test	p =5.0549e-08 and p = 2.2116e-12 for differences in no tail bend responses between wild type and mutants and heterozygotes and mutants respectively

Figure 3C	-	Chi-square test	p = 2.2687e-06 and p = 0.0026 for differences in ipsilateral tail bend responses in wild type and mutant and heterozygotes and mutants respectively
Figure 3E	Non-normal	Kruskal Wallis; Mann-Whitney for between group comparisons	p=1.0831e-06; p = 2.5258e-05 for differences in latencies between wild type and mutants, p = 8.7877e-06 for differences between heterozygotes and mutants.
Figure 3F	Non-normal	Kruskal Wallis; Mann-Whitney for between group comparisons	p = 0.0004; p = 0.0010 for differences in latencies between wild type and mutants, p = 0.0010 for differences between heterozygotes and mutants
Figure 3G	Non-normal	Kruskal Wallis; Mann-Whitney for between group comparisons	p=0.0004; p= 6.3799e-04 for differences in CV of latencies between wild type and mutants, p= 5.7969e-04 for differences in CV between heterozygote and mutants

Figure 3H	Non-normal	Kruskal Wallis; Mann-Whitney for between group comparisons	p= 0.0413; p = 0.9107 for differences in tail bend angle between wild type and mutants, p =0.01 for differences between heterozygotes and mutants
Figure 4C	-	Chi-square test	p=0.0111 for differences in contralateral tail bend responses between wildtype and mutants
Figure 4C	-	Chi-square test	p=1.4745e-06 for differences in no tail bend responses between wild type and mutants
Figure 4C	-	Chi-square test	p= 0.3513 for differences in ipsilateral tail bend responses between wild type and mutants
Figure 4D	Normal	t-test	p= 0.0044 for differences in cdf of latencies between wild type and mutants
Figure 4E	Normal	t-test	p= 0.0676 for differences in CV of latencies between wild type and mutants
Figure 4F	Normal	t-test	p=0.0625 for differences in tail bend angle between wild type and mutants

Figure 5D	Non-normal	Mann-Whitney U test	p=0.0079 for differences in probability of calcium activity in M-cell between wild type and mutants
Figure 5E	Non-normal	Mann-Whitney U test	p= 1.4939e-13 for differences in peak ΔF/F between wild type and mutants
Figure 5F	Non-normal	Mann-Whitney U test	p=0.119 for differences in coefficient of variation in ΔF/F between wild type and mutants
Figure 6D	Non-normal	Mann-Whitney U test	p=0.0196 for differences in threshold between wild type and mutants
Figure 6G	Non-normal	Mann-Whitney U test	p= 2.8355e-04 for differences in peak ΔF/F between wild type and mutants
Figure 6H	Non-normal	Wilcoxon signed rank test	p=1 for before and after comparison for WT, p=0.5 for before and after comparison for mutants
Figure 6I	Normal	t-test	p= 0.1596 for before and after comparison for WT, p= 0.6467 for before and after comparison for mutants

732

Reference:

Bedell VM, Wang Y, Campbell JM, Poshusta TL, Starker CG, Krug Ii RG, Tan W, Penheiter SG, Ma AC, Leung AYH, Fahrenkrug SC, Carlson DF, Voytas DF, Clark KJ, Essner JJ, Ekker SC. 2012. In vivo genome editing using a high-efficiency TALEN system. *Nature* **491**:114–118. doi:10.1038/nature11537

Bedogni F, Hodge RD, Nelson BR, Frederick EA, Shiba N, Daza RA, Hevner RF. 2010. Autism susceptibility candidate 2 (Auts2) encodes a nuclear protein expressed in developing brain regions implicated in autism neuropathology. *Gene Expression Patterns* **10**:9–15. doi:10.1016/j.gep.2009.11.005

Beunders G, Voorhoeve E, Golzio C, Pardo LM, Rosenfeld JA, Talkowski ME, Simonic I, Lionel AC, Vergult S, Pyatt RE, van de Kamp J, Nieuwint A, Weiss MM, Rizzu P, Verwer LENI, van Spaendonk RML, Shen Y, Wu B, Yu T, Yu Y, Chiang C, Gusella JF, Lindgren AM, Morton CC, van Binsbergen E, Bulk S, van Rossem E, Vanakker O, Armstrong R, Park S-M, Greenhalgh L, Maye U, Neill NJ, Abbott KM, Sell S, Ladda R, Farber DM, Bader PI, Cushing T, Drautz JM, Konczal L, Nash P, de Los Reyes E, Carter MT, Hopkins E, Marshall CR, Osborne LR, Gripp KW, Thrush DL, Hashimoto S, Gastier-Foster JM, Astbury C, Ylstra B, Meijers-Heijboer H, Posthuma D, Menten B, Mortier G, Scherer SW, Eichler EE, Girirajan S, Katsanis N, Groffen AJ, Sistermans EA. 2013. Exonic Deletions in AUTS2 Cause a Syndromic Form of Intellectual Disability and Suggest a Critical Role for the C Terminus. *The American Journal of Human Genetics* **92**:210–220. doi:10.1016/j.ajhg.2012.12.011

Bourgeron T. 2015. From the genetic architecture to synaptic plasticity in autism spectrum disorder. *Nature Reviews Neuroscience* **16**:551–563. doi:10.1038/nrn3992

759 Brewster DL, Ali DW. 2013. Expression of the voltage-gated potassium channel
760 subunit Kv1.1 in embryonic zebrafish Mauthner cells. *Neuroscience Letters*
761 **539**:54–59. doi:10.1016/j.neulet.2013.01.042
762 Burgess HA, Granato M. 2007. Sensorimotor Gating in Larval Zebrafish. *J Neurosci*
763 **27**:4984–4994. doi:10.1523/JNEUROSCI.0615-07.2007
764 Burgess HA, Johnson SL, Granato M. 2009. Unidirectional startle responses and
765 disrupted left-right co-ordination of motor behaviors in robo3 mutant zebrafish.
766 *Genes Brain Behav* **8**:500–511. doi:10.1111/j.1601-183X.2009.00499.x
767 De Rubeis S, He X, Goldberg AP, Poultney CS, Samocha K, Ercument Cicek A, Kou
768 Y, Liu L, Fromer M, Walker S, Singh T, Klei L, Kosmicki J, Fu S-C, Aleksic B,
769 Biscaldi M, Bolton PF, Brownfeld JM, Cai J, Campbell NG, Carracedo A,
770 Chahrour MH, Chiocchetti AG, Coon H, Crawford EL, Crooks L, Curran SR,
771 Dawson G, Duketis E, Fernandez BA, Gallagher L, Geller E, Guter SJ, Sean
772 Hill R, Ionita-Laza I, Jimenez Gonzalez P, Kilpinen H, Klauck SM, Kolevzon A,
773 Lee I, Lei J, Lehtimäki T, Lin C-F, Ma'ayan A, Marshall CR, McInnes AL,
774 Neale B, Owen MJ, Ozaki N, Parellada M, Parr JR, Purcell S, Puura K,
775 Rajagopalan D, Rehnström K, Reichenberg A, Sabo A, Sachse M, Sanders
776 SJ, Schafer C, Schulte-Rüther M, Skuse D, Stevens C, Szatmari P,
777 Tammimies K, Valladares O, Voran A, Wang L-S, Weiss LA, Jeremy Willsey
778 A, Yu TW, Yuen RKC, Cook EH, Freitag CM, Gill M, Hultman CM, Lehner T,
779 Palotie A, Schellenberg GD, Sklar P, State MW, Sutcliffe JS, Walsh CA,
780 Scherer SW, Zwick ME, Barrett JC, Cutler DJ, Roeder K, Devlin B, Daly MJ,
781 Buxbaum JD. 2014. Synaptic, transcriptional and chromatin genes disrupted
782 in autism. *Nature* **515**:209–215. doi:10.1038/nature13772

783 Desai NS. 2003. Homeostatic plasticity in the CNS: synaptic and intrinsic forms.
784 *Journal of Physiology-Paris*, Neuroscience and Computation **97**:391–402.
785 doi:10.1016/j.jphysparis.2004.01.005
786 Eaton RC, Bombardieri RA, Meyer DL. 1977. The Mauthner-initiated startle response
787 in teleost fish. *J Exp Biol* **66**:65–81.
788 Eaton RC, Farley RD. 1975. Mauthner neuron field potential in newly hatched larvae
789 of the zebra fish. *J Neurophysiol* **38**:502–512. doi:10.1152/jn.1975.38.3.502
790 Eaton RC, Lavender WA, Wieland CM. 1981. Identification of Mauthner-initiated
791 response patterns in goldfish: Evidence from simultaneous cinematography
792 and electrophysiology. *J Comp Physiol* **144**:521–531.
793 doi:10.1007/BF01326837
794 Eaton RC, Lee RKK, Foreman MB. 2001. The Mauthner cell and other identified
795 neurons of the brainstem escape network of fish. *Progress in Neurobiology*
796 **63**:467–485. doi:10.1016/S0301-0082(00)00047-2
797 Eaton RC, Nissanov J, Wieland CM. 1984. Differential activation of Mauthner and
798 non-Mauthner startle circuits in the zebrafish: Implications for functional
799 substitution. *J Comp Physiol* **155**:813–820. doi:10.1007/BF00611598
800 Fetcho JR. 1991. Spinal network of the Mauthner cell. *Brain Behav Evol* **37**:298–316.
801 doi:10.1159/000114367
802 Gahtan E, Baier H. 2004. Of lasers, mutants, and see-through brains: functional
803 neuroanatomy in zebrafish. *J Neurobiol* **59**:147–161. doi:10.1002/neu.20000
804 Gao Z, Lee P, Stafford JM, von Schimmelmann M, Schaefer A, Reinberg D. 2014.
805 An AUTS2-Polycomb complex activates gene expression in the CNS. *Nature*
806 **516**:349–354. doi:10.1038/nature13921

807 Granato M, Eeden FJ van, Schach U, Trowe T, Brand M, Furutani-Seiki M, Haffter P,
808 Hammerschmidt M, Heisenberg CP, Jiang YJ, Kane DA, Kelsh RN, Mullins
809 MC, Odenthal J, Nusslein-Volhard C. 1996. Genes controlling and mediating
810 locomotion behavior of the zebrafish embryo and larva. *Development*
811 **123**:399–413.
812 Heyes S, Pratt WS, Rees E, Dahimene S, Ferron L, Owen MJ, Dolphin AC. 2015.
813 Genetic disruption of voltage-gated calcium channels in psychiatric and
814 neurological disorders. *Prog Neurobiol* **134**:36–54.
815 doi:10.1016/j.pneurobio.2015.09.002
816 Hori K, Hoshino M. 2017. Neuronal Migration and AUTS2 Syndrome. *Brain Sciences*
817 **7**:54. doi:10.3390/brainsci7050054
818 Hori K, Nagai T, Shan W, Sakamoto A, Taya S, Hashimoto R, Hayashi T, Abe M,
819 Yamazaki M, Nakao K, Nishioka T, Sakimura K, Yamada K, Kaibuchi K,
820 Hoshino M. 2014. Cytoskeletal regulation by AUTS2 in neuronal migration
821 and neuritogenesis. *Cell Rep* **9**:2166–2179. doi:10.1016/j.celrep.2014.11.045
822 Hori K, Yamashiro K, Nagai T, Shan W, Egusa SF, Shimaoka K, Kuniishi H,
823 Sekiguchi M, Go Y, Tatsumoto S, Yamada Mitsuyo, Shiraishi R, Kanno K,
824 Miyashita S, Sakamoto A, Abe M, Sakimura K, Sone M, Sohya K, Kunugi H,
825 Wada K, Yamada Mitsuhiko, Yamada K, Hoshino M. 2020. AUTS2 Regulation
826 of Synapses for Proper Synaptic Inputs and Social Communication. *iScience*
827 **23**:101183. doi:10.1016/j.isci.2020.101183
828 Ibata K, Sun Q, Turrigiano GG. 2008. Rapid Synaptic Scaling Induced by Changes in
829 Postsynaptic Firing. *Neuron* **57**:819–826. doi:10.1016/j.neuron.2008.02.031
830 Jain RA, Wolman MA, Marsden KC, Nelson JC, Shoenhard H, Echeverry FA, Szi C,
831 Bell H, Skinner J, Cobbs EN, Sawada K, Zamora AD, Pereda AE, Granato M.

2018. A Forward Genetic Screen in Zebrafish Identifies the G-Protein-Coupled Receptor CaSR as a Modulator of Sensorimotor Decision Making. *Curr Biol* **28**:1357-1369.e5. doi:10.1016/j.cub.2018.03.025

Kalscheuer VM, FitzPatrick D, Tommerup N, Bugge M, Niebuhr E, Neumann LM, Tzschach A, Shoichet SA, Menzel C, Erdogan F, Arkesteijn G, Ropers H-H, Ullmann R. 2007. Mutations in autism susceptibility candidate 2 (AUTS2) in patients with mental retardation. *Hum Genet* **121**:501–509. doi:10.1007/s00439-006-0284-0

Kimmel CB, Patterson J, Kimmel RO. 1974. The development and behavioral characteristics of the startle response in the zebra fish. *Developmental Psychobiology* **7**:47–60. doi:10.1002/dev.420070109

Kimmel CB, Powell SL, Metcalfe WK. 1982. Brain neurons which project to the spinal cord in young larvae of the zebrafish. *Journal of Comparative Neurology* **205**:112–127. doi:10.1002/cne.902050203

Kohashi T, Nakata N, Oda Y. 2012. Effective Sensory Modality Activating an Escape Triggering Neuron Switches during Early Development in Zebrafish. *J Neurosci* **32**:5810–5820. doi:10.1523/JNEUROSCI.6169-11.2012

Kohashi T, Oda Y. 2008. Initiation of Mauthner- or Non-Mauthner-Mediated Fast Escape Evoked by Different Modes of Sensory Input. *J Neurosci* **28**:10641–10653. doi:10.1523/JNEUROSCI.1435-08.2008

Kondrychyn I, Robra L, Thirumalai V. 2017. Transcriptional Complexity and Distinct Expression Patterns of auts2 Paralogs in Danio rerio. *G3 (Bethesda)* **7**:2577–2593. doi:10.1534/g3.117.042622

855 Korn H, Faber DS. 2005. The Mauthner Cell Half a Century Later: A Neurobiological
856 Model for Decision-Making? *Neuron* **47**:13–28.
857 doi:10.1016/j.neuron.2005.05.019
858 Krey JF, Dolmetsch RE. 2007. Molecular mechanisms of autism: a possible role for
859 Ca2+ signaling. *Current Opinion in Neurobiology*, Development **17**:112–119.
860 doi:10.1016/j.conb.2007.01.010
861 Kron M, Howell CJ, Adams IT, Ransbottom M, Christian D, Ogier M, Katz DM. 2012.
862 Brain Activity Mapping in Mecp2 Mutant Mice Reveals Functional Deficits in
863 Forebrain Circuits, Including Key Nodes in the Default Mode Network, that are
864 Reversed with Ketamine Treatment. *J Neurosci* **32**:13860–13872.
865 doi:10.1523/JNEUROSCI.2159-12.2012
866 Lee E, Lee J, Kim E. 2017. Excitation/Inhibition Imbalance in Animal Models of
867 Autism Spectrum Disorders. *Biological Psychiatry* **81**:838–847.
868 doi:10.1016/j.biopsych.2016.05.011
869 Liu KS, Fetcho JR. 1999. Laser Ablations Reveal Functional Relationships of
870 Segmental Hindbrain Neurons in Zebrafish. *Neuron* **23**:325–335.
871 doi:10.1016/S0896-6273(00)80783-7
872 Lorent K, Liu KS, Fetcho JR, Granato M. 2001. The zebrafish space cadet gene
873 controls axonal pathfinding of neurons that modulate fast turning movements.
874 *Development* **128**:2131–2142.
875 Lory P, Nicole S, Monteil A. 2020. Neuronal Cav3 channelopathies: recent progress
876 and perspectives. *Pflugers Arch - Eur J Physiol* **472**:831–844.
877 doi:10.1007/s00424-020-02429-7

878 Marquart GD, Tabor KM, Bergeron SA, Briggman KL, Burgess HA. 2019. Prepontine
879 non-giant neurons drive flexible escape behavior in zebrafish. *PLOS Biology*
880 **17**:e3000480. doi:10.1371/journal.pbio.3000480
881 Marsden KC, Jain RA, Wolman MA, Echeverry FA, Nelson JC, Hayer KE, Miltenberg
882 B, Pereda AE, Granato M. 2018. A Cyfip2-Dependent Excitatory Interneuron
883 Pathway Establishes the Innate Startle Threshold. *Cell Rep* **23**:878–887.
884 doi:10.1016/j.celrep.2018.03.095
885 Meeker ND, Hutchinson SA, Ho L, Trede NS. 2007. Method for isolation of PCR-
886 ready genomic DNA from zebrafish tissues. *BioTechniques* **43**:610–614.
887 doi:10.2144/000112619
888 Metcalfe WK, Mendelson B, Kimmel CB. 1986. Segmental homologies among
889 reticulospinal neurons in the hindbrain of the zebrafish larva. *Journal of*
890 *Comparative Neurology* **251**:147–159. doi:10.1002/cne.902510202
891 Minshew NJ, Keller TA. 2010. "The Nature of Brain Dysfunction in Autism: Functional
892 Brain Imaging Studies." *Curr Opin Neurol* **23**:124–130.
893 doi:10.1097/WCO.0b013e32833782d4
894 Nakayama H, Oda Y. 2004. Common Sensory Inputs and Differential Excitability of
895 Segmentally Homologous Reticulospinal Neurons in the Hindbrain. *J Neurosci*
896 **24**:3199–3209. doi:10.1523/JNEUROSCI.4419-03.2004
897 Nelson SB, Valakh V. 2015. Excitatory/Inhibitory Balance and Circuit Homeostasis in
898 Autism Spectrum Disorders. *Neuron* **87**:684–698.
899 doi:10.1016/j.neuron.2015.07.033
900 Oksenberg N, Ahituv N. 2013. The role of AUTS2 in neurodevelopment and human
901 evolution. *Trends in Genetics* **29**:600–608. doi:10.1016/j.tig.2013.08.001

902 Oksenberg N, Haliburton GDE, Eckalbar WL, Oren I, Nishizaki S, Murphy K, Pollard
903 KS, Birnbaum RY, Ahituv N. 2014. Genome-wide distribution of Auts2 binding
904 localizes with active neurodevelopmental genes. *Translational Psychiatry*
905 **4**:e431–e431. doi:10.1038/tp.2014.78
906 Roy B, Ali DW (2014) Multiple types of GABAA responses identified from zebrafish
907 Mauthner cells. Neuroreport 25:1232–1236.
908 Rubenstein JLR, Merzenich MM. 2003. Model of autism: increased ratio of
909 excitation/inhibition in key neural systems. *Genes, Brain and Behavior* **2**:255–
910 267. doi:10.1034/j.1601-183X.2003.00037.x
911 Russo D, Della Ragione F, Rizzo R, Sugiyama E, Scalabrì F, Hori K, Capasso S,
912 Sticco L, Fioriniello S, De Gregorio R, Granata I, Guarracino MR, Maglione V,
913 Johannes L, Bellenchi GC, Hoshino M, Setou M, D'Esposito M, Luini A,
914 D'Angelo G. 2018. Glycosphingolipid metabolic reprogramming drives neural
915 differentiation. *The EMBO Journal* **37**:e97674. doi:10.15252/embj.201797674
916 Sanjana NE, Cong L, Zhou Y, Cunniff MM, Feng G, Zhang F. 2012. A transcription
917 activator-like effector toolbox for genome engineering. *Nat Protoc* **7**:171–192.
918 doi:10.1038/nprot.2011.431
919 Schaukowitch K, Reese AL, Kim S-K, Kilaru G, Joo J-Y, Kavalali ET, Kim T-K. 2017.
920 An Intrinsic Transcriptional Program Underlying Synaptic Scaling during
921 Activity Suppression. *Cell Rep* **18**:1512–1526.
922 doi:10.1016/j.celrep.2017.01.033
923 Schindelin J, Arganda-Carreras I, Frise E, Kaynig V, Longair M, Pietzsch T,
924 Preibisch S, Rueden C, Saalfeld S, Schmid B, Tinevez J-Y, White DJ,
925 Hartenstein V, Eliceiri K, Tomancak P, Cardona A. 2012. Fiji: an open-source

platform for biological-image analysis. *Nat Methods* **9**:676–682. doi:10.1038/nmeth.2019

Sillar KT. 2009. Mauthner cells. *Current Biology* **19**:R353–R355. doi:10.1016/j.cub.2009.02.025

Sohal VS, Rubenstein JLR. 2019. Excitation-inhibition balance as a framework for investigating mechanisms in neuropsychiatric disorders. *Molecular Psychiatry* **24**:1248–1257. doi:10.1038/s41380-019-0426-0

Sultana R, Yu C-E, Yu J, Munson J, Chen D, Hua W, Estes A, Cortes F, de la Barra F, Yu D, Haider ST, Trask BJ, Green ED, Raskind WH, Disteche CM, Wijsman E, Dawson G, Storm DR, Schellenberg GD, Villacres EC. 2002. Identification of a Novel Gene on Chromosome 7q11.2 Interrupted by a Translocation Breakpoint in a Pair of Autistic Twins. *Genomics* **80**:129–134. doi:10.1006/geno.2002.6810

Sztainberg Y, Zoghbi HY. 2016. Lessons learned from studying syndromic autism spectrum disorders. *Nature Neuroscience* **19**:1408–1417. doi:10.1038/nn.4420

Takahashi M, Narushima M, Oda Y (2002) In Vivo Imaging of Functional Inhibitory Networks on the Mauthner Cell of Larval Zebrafish. J Neurosci 22:3929–3938.

Turrigiano GG, Leslie KR, Desai NS, Rutherford LC, Nelson SB. 1998. Activity-dependent scaling of quantal amplitude in neocortical neurons. *Nature* **391**:892–896. doi:10.1038/36103

Turrigiano GG, Nelson SB. 2004. Homeostatic plasticity in the developing nervous system. *Nat Rev Neurosci* **5**:97–107. doi:10.1038/nrn1327

Wang Q, Geng Z, Gong Y, Warren K, Zheng H, Imamura Y, Gao Z. 2018. WDR68 is essential for the transcriptional activation of the PRC1-AUTS2 complex and

neuronal differentiation of mouse embryonic stem cells. *Stem Cell Research* **33**:206–214. doi:10.1016/j.scr.2018.10.023

Watanabe T, Shimazaki T, Mishiro A, Suzuki T, Hirata H, Tanimoto M, Oda Y. 2013. Coexpression of auxiliary Kvβ2 subunits with Kv1.1 channels is required for developmental acquisition of unique firing properties of zebrafish Mauthner cells. *Journal of Neurophysiology* **111**:1153–1164. doi:10.1152/jn.00596.2013

Watanabe T, Shimazaki T, Oda Y. 2017. Coordinated Expression of Two Types of Low-Threshold K+ Channels Establishes Unique Single Spiking of Mauthner Cells among Segmentally Homologous Neurons in the Zebrafish Hindbrain. *eNeuro* **4**. doi:10.1523/ENEURO.0249-17.2017

Westerfield M. 2000. The Zebrafish Book: A Guide for the Laboratory Use of Zebrafish (Danio Rerio). University of Oregon Press.

Wolman M, Granato M. 2012. Behavioral Genetics in Larval Zebrafish: Learning from the Young. *Dev Neurobiol* **72**:366–372. doi:10.1002/dneu.20872

Wolman MA, Jain RA, Marsden KC, Bell H, Skinner J, Hayer KE, Hogenesch JB, Granato M. 2015. A Genome-wide Screen Identifies PAPP-AA-Mediated IGFR Signaling as a Novel Regulator of Habituation Learning. *Neuron* **85**:1200–1211. doi:10.1016/j.neuron.2015.02.025

Zottoli SJ. 1977. Correlation of the startle reflex and Mauthner cell auditory responses in unrestrained goldfish. *J Exp Biol* **66**:243–254.

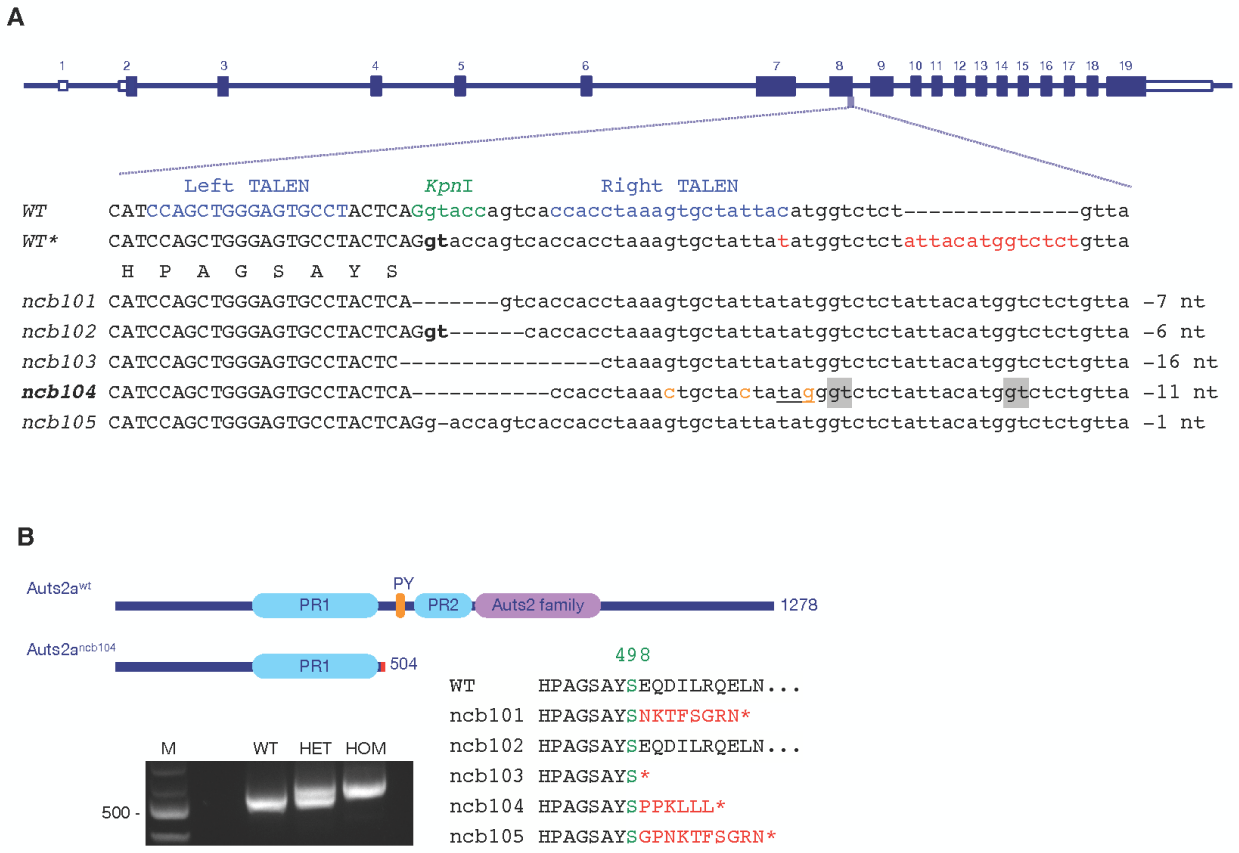

Figure 1.

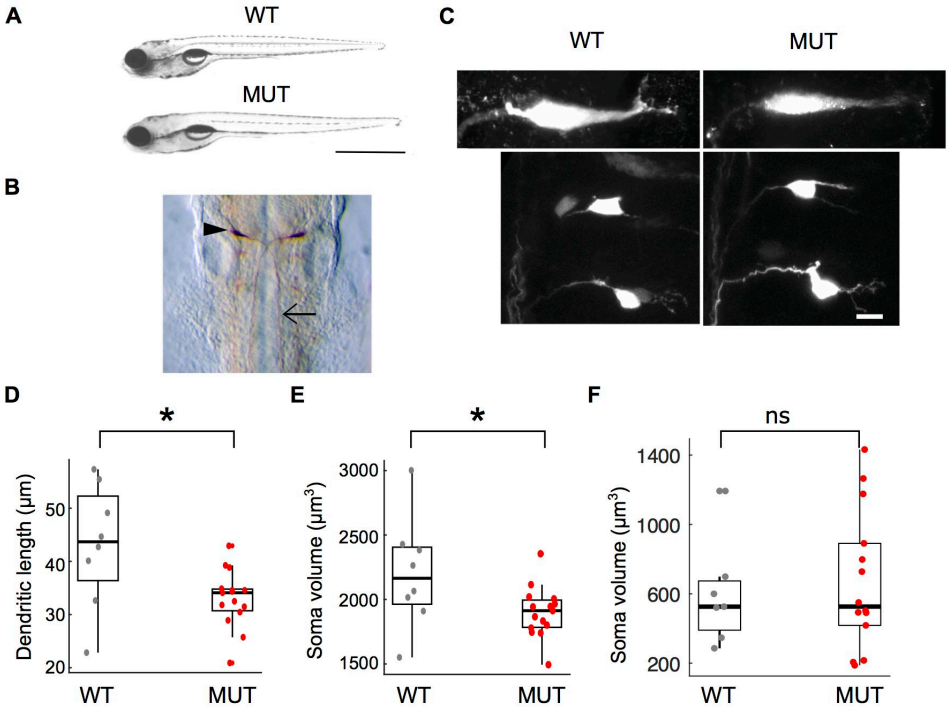

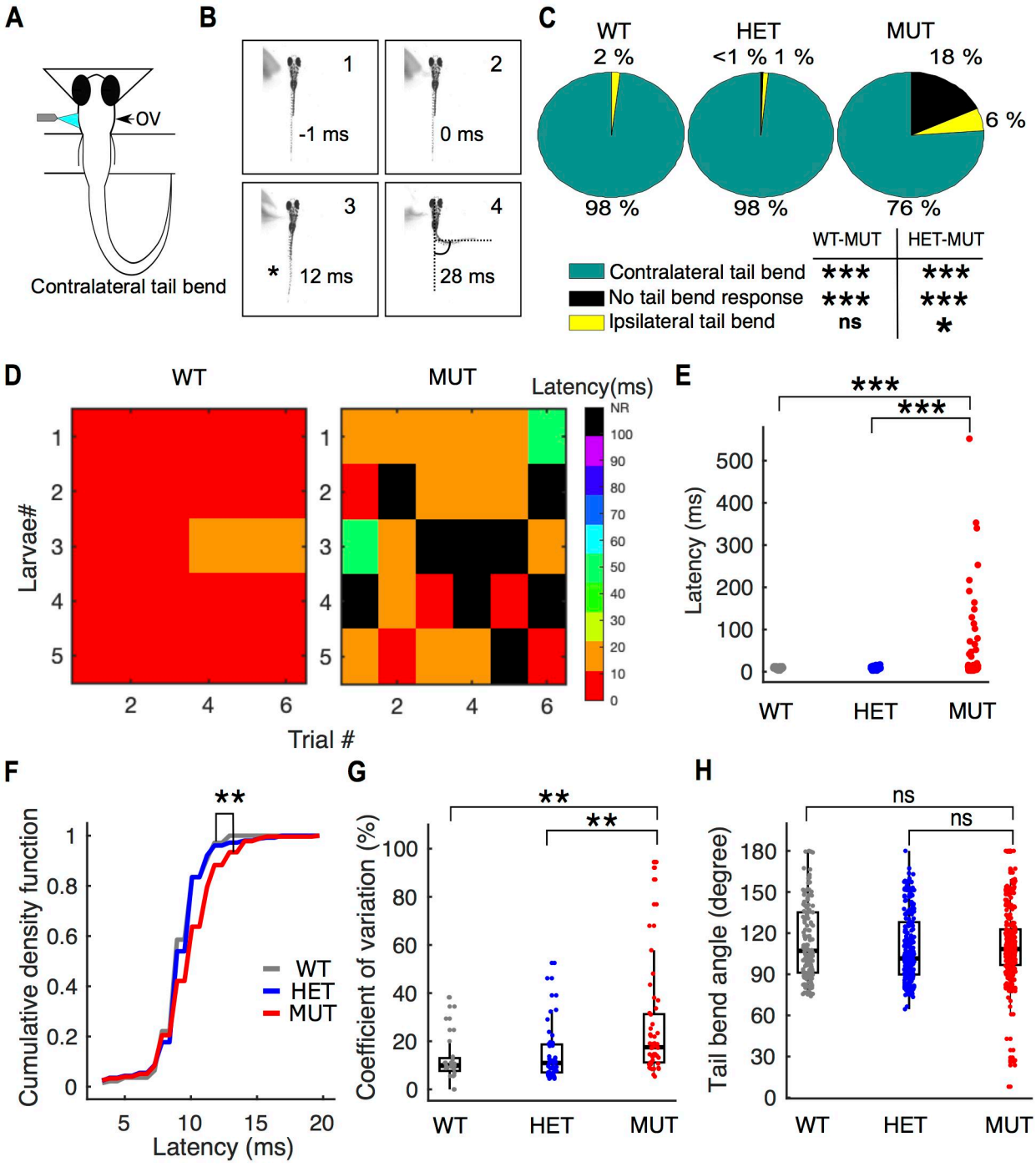

Figure 2.

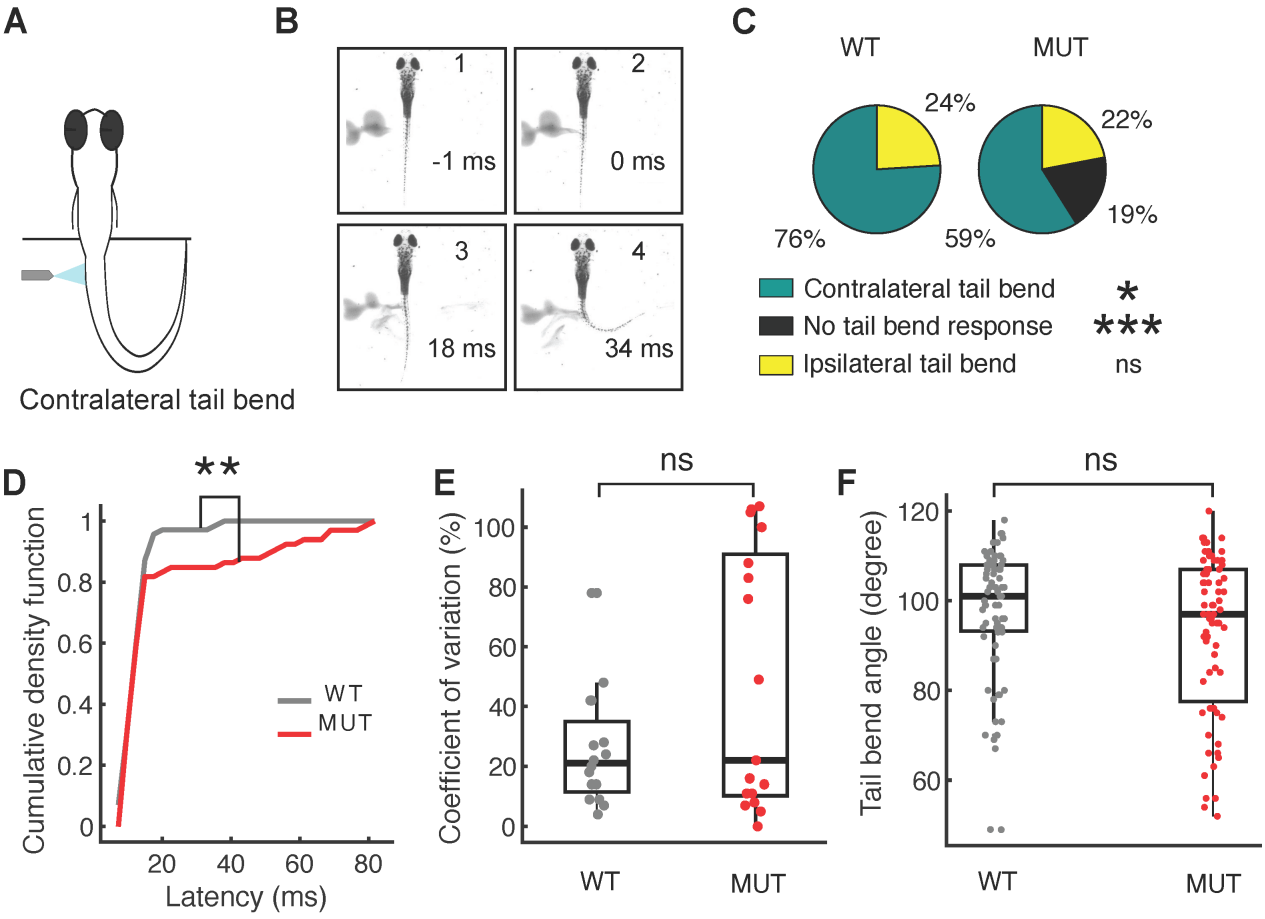

Figure 4.

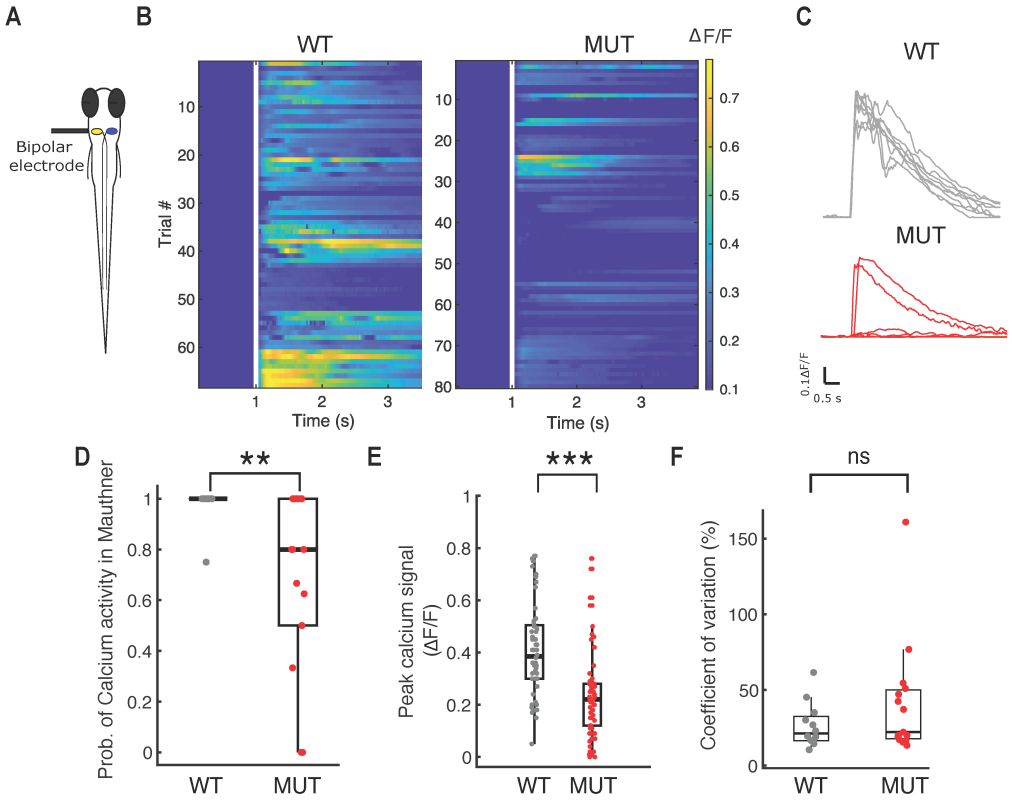

Figure 5.

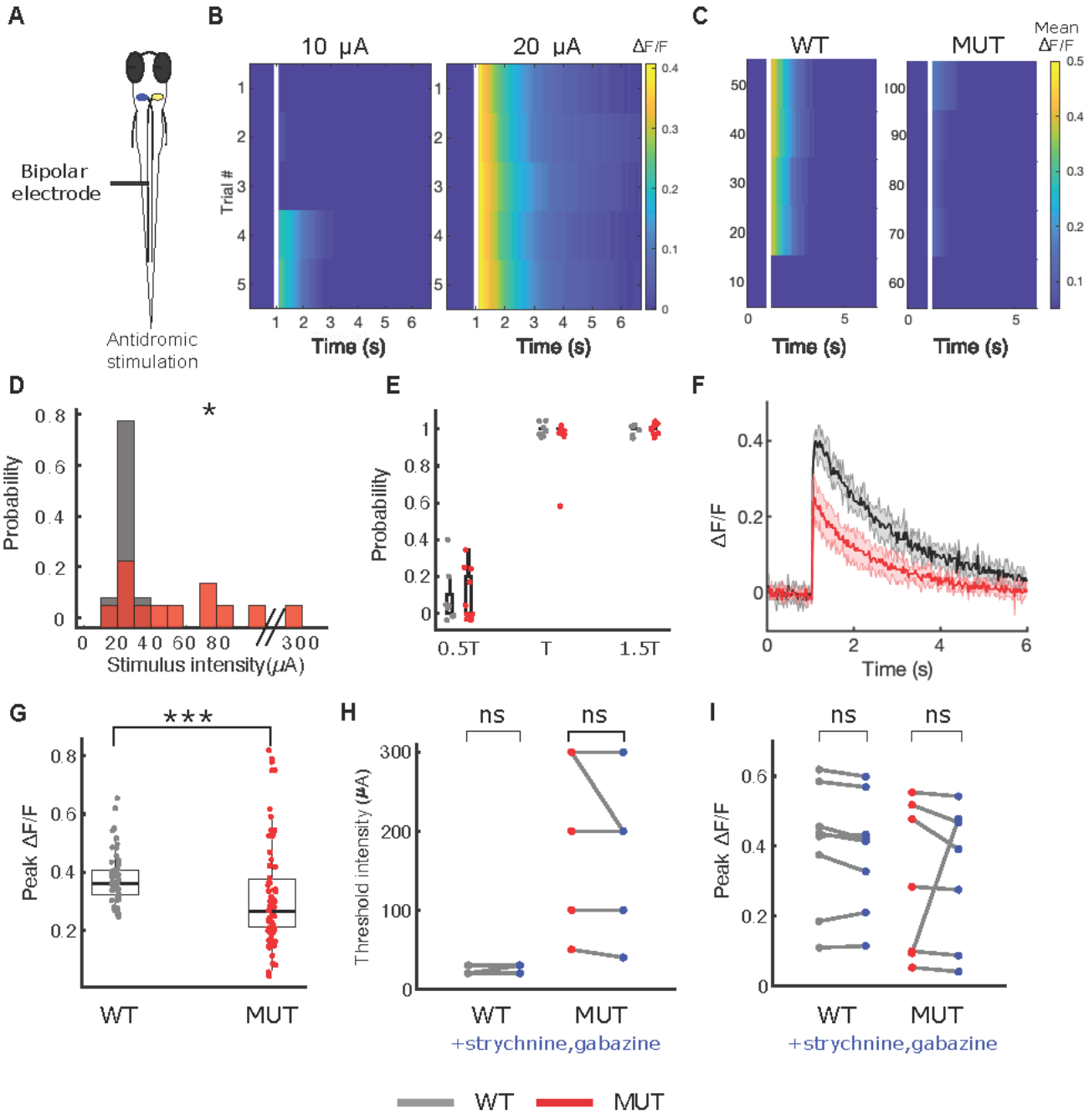

Figure 6.

-

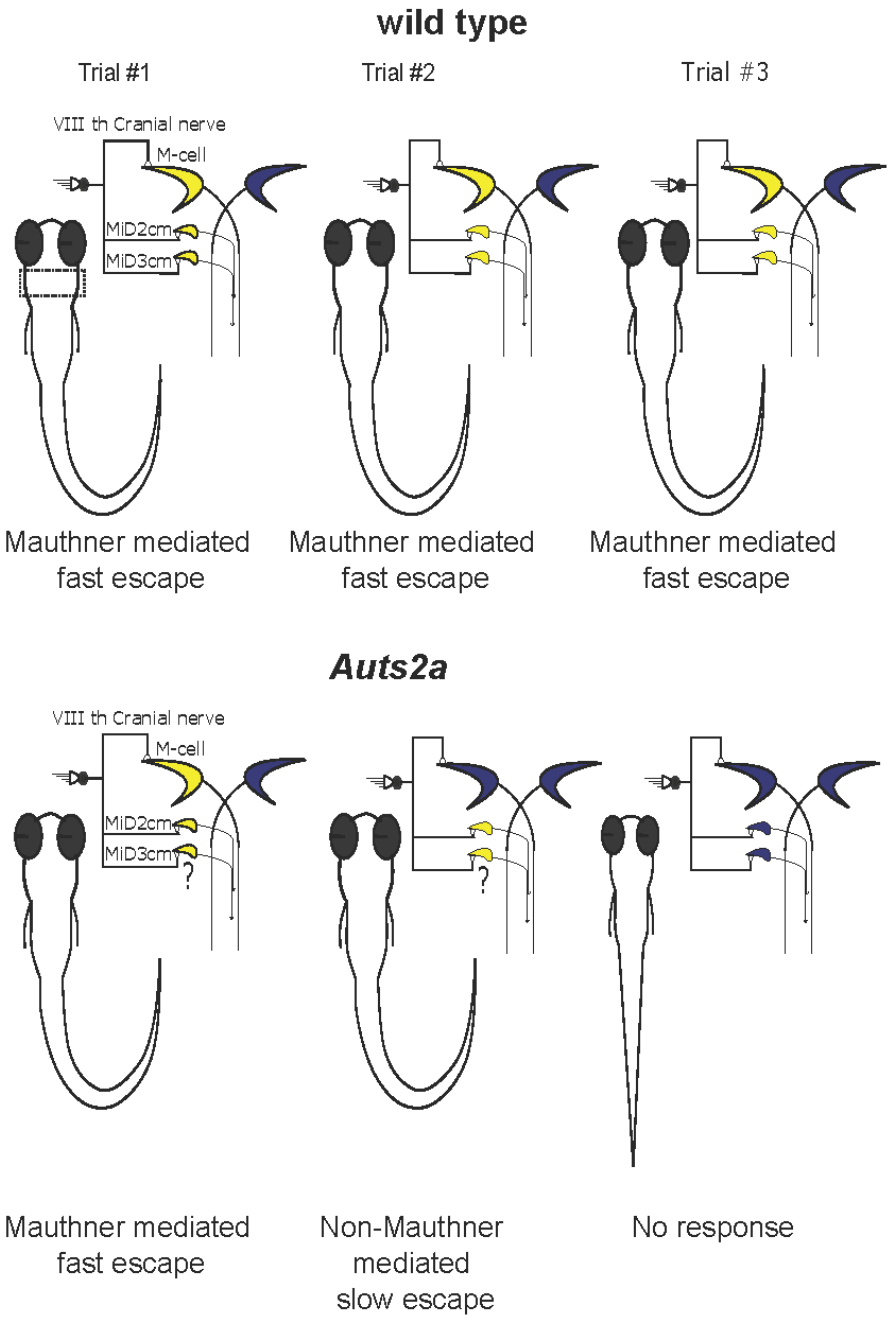

Figure 7.